

Title: *PARaDIM – A PHITS-based Monte Carlo tool for internal dosimetry with tetrahedral mesh computational phantoms*

Running title: *PARADIM – A PHITS-based dosimetry tool*

Authors:

Lukas M. Carter^{*1}, Troy M. Crawford^{*2}, Tatsuhiko Sato^{3,4}, Takuya Furuta³, Chansoo Choi⁵, Chan Hyeon Kim⁵, Justin L. Brown⁶, Wesley E. Bolch⁶, Pat B. Zanzonico⁷, Jason S. Lewis^{1,8}

Affiliations:

¹Department of Radiology, Program in Pharmacology and the Radiochemistry and Molecular Imaging Probes Core, Memorial Sloan Kettering Cancer Center, New York, NY, USA

²Department of Physics, University of Rhode Island, Kingston, RI, USA

³Japan Atomic Energy Agency, Ibaraki, Japan

⁴Research Center for Nuclear Physics, Osaka University, Osaka, Japan

⁵Department of Nuclear Engineering, Hanyang University, Seoul, Korea

⁶J. Crayton Pruitt Family Department of Biomedical Engineering, University of Florida, Gainesville, FL, USA

⁷Department of Medical Physics, Memorial Sloan Kettering Cancer Center, New York, NY, USA

⁸Department of Radiology and Department of Pharmacology, Weill Cornell Medical College, New York, NY, USA

^{*}Authors contributed equally to the manuscript

First Author: Lukas M. Carter

417 East 68th Street, New York, NY, USA. P: (646)888-3081 E: carterl1@mskcc.org

Corresponding author: Jason S. Lewis

417 East 68th Street, New York, NY, USA. P: (646)888-3038 E: lewisj2@mskcc.org

ABSTRACT

Mesh-type and voxel-based computational phantoms comprise the current state-of-the-art for internal dose assessment via Monte Carlo simulations, but excel in different aspects, with mesh-type phantoms offering advantages over their voxel counterparts in terms of their flexibility and realistic representation of detailed patient- or subject-specific anatomy. We have developed PARaDIM, a freeware application for implementing tetrahedral mesh-type phantoms in absorbed dose calculations via the Particle and Heavy Ion Transport code System (PHITS). It considers all medically relevant radionuclides including alpha, beta, gamma, positron, and Auger/conversion electron emitters, and handles calculation of mean dose to individual regions, as well as 3D dose distributions for visualization and analysis in a variety of medical imaging softwares. This work describes the development of PARaDIM, documents the measures taken to test and validate its performance, and presents examples to illustrate its uses. **Methods:** Human, small animal, and cell-level dose calculations were performed with PARaDIM and the results compared with those of widely accepted dosimetry programs and literature data. Several tetrahedral phantoms were developed or adapted using computer-aided modeling techniques for these comparisons. **Results:** For human dose calculations, agreement of PARaDIM with OLINDA 2.0 was good – within 10-20% for most organs – despite geometric differences among the phantoms tested. Agreement with MIRDcell for cell-level S-value calculations was within 5% in most cases. **Conclusion:** PARaDIM extends the use of Monte Carlo dose calculations to the broader community in nuclear medicine by providing a user-friendly graphical user interface for calculation setup and execution. PARaDIM leverages the enhanced anatomical realism provided by advanced computational reference phantoms or bespoke image-derived phantoms to enable improved assessments of radiation doses in a variety of radiopharmaceutical use cases, research, and preclinical development.

KEY WORDS

PARaDIM, PHITS, dosimetry, tetrahedral mesh, phantom

INTRODUCTION

Radiopharmaceutical use demands consideration of dosimetric implications in clinical use cases, preclinical animal studies, and in cell-based assays. For human use, accurate dosimetry is a requisite for meaningful risk projection from low-dose imaging procedures, as well as for reliable pre-radionuclide therapy dose planning, response assessment, and characterization of potential toxicities. In the preclinical setting, the considerations are similar but more nuanced – for example, the high activities per unit mass utilized in preclinical PET and SPECT investigations generally deliver elevated absorbed doses to small animal hosts and thus have the potential to induce radiotoxicity, alter gene expression, or present other biological anomalies complicating interpretation of the scientific output. Tools have been developed to perform organ-level dosimetry in humans and mice(1), but generally implement a limited set of phantoms and have limited or no provisions for assessment of non-uniform dose deposition within phantom regions; alternatively, several image-based dosimetry tools exist(2–5), but their accuracy is dependent on the quantitative accuracy of PET/SPECT imaging – a versatile methodology that combines advantages of both approaches would be beneficial. Finally, the dose to cell components has been shown to be sensitive to the cell size/shape and location of the decay site(6,7) particularly for radiations with high linear energy transfer (LET). MIRDcell(8) has been a reliable tool for cell-level dose assessment for some time, and models dose to single cells or cell clusters. However, all cells within MIRDcell are modeled as concentric spheres, which in certain cases can be limiting. Considering the increasing emphasis on high-LET radionuclide therapies, a practical option for cell-level dose modeling to irregular cell geometries would be timely.

We have developed PARaDIM (PHITS-based Application for Radionuclide Dosimetry In Meshes; pronounced “paradigm”), a program which employs the Particle and Heavy Ion Transport code System (PHITS v3.07 or later)(9,10) for dose computation. No knowledge of the PHITS source code, input file format, or parameter syntax is required for its use. Similar to other

programs for mean organ-level dose assessment based on pre-computed S-values, PARaDIM implements a user-friendly graphical user interface for input of time-integrated activity coefficients(11), and generates organ-level mean absorbed doses under the assumption that the activity is uniformly distributed throughout each source region. Additionally, PARaDIM provides voxelized 3D dose maps at user-specified resolution, supporting assessment of heterogeneity of dose deposition. PARaDIM supports cell-level dosimetry based on modeling single cells or cell clusters of arbitrary shape/spacing and with arbitrary components through characterization of cells and clusters as a tetrahedral mesh.

It is our expectation that PARaDIM will allow researchers in preclinical nuclear medicine to make improved assessments of radiation dose in small-animal imaging and therapy studies, cell-based assays, as well as provide more accurate projections of absorbed dose to potential patients of various body habitus in support of radiopharmaceutical development and investigational new drug (IND) applications. For human dosimetry, PARaDIM will provide a robust supplement to image-based methods, primarily offering a level of non-uniform dose assessment applicable to patient populations, and personalized output from patient-specific phantoms derived from tomographic image data.

MATERIALS AND METHODS

Code Development and Functionality

PHITS is a multipurpose particle-transport code, handling transport of virtually all known particle types for applications in medical physics and radiation protection among other fields. PARaDIM assembles user-specified phantom geometry, source definition, and simulation parameters into a PHITS-compatible input file for execution (Fig. 1). Following submission of a simulation from PARaDIM, PHITS initiates and transports the various particle and photon

emissions within the phantom geometry, and tallies energy deposition within phantom regions or in a voxel grid.

For all simulations, PARaDIM utilizes tetrahedral mesh-type computational phantoms(12–17); ref. (16) provides a detailed discussion of computation speeds and memory requirements of this phantom format relative to voxel phantoms. The PHITS code was recently updated to support such phantoms, and their use within PHITS for absorbed dose calculations has been well-validated(12). A library of tetrahedral phantoms has been provided with PARaDIM, enumerated in Table 1; phantoms can be accessed through PARaDIM's 'Phantom Selection' module (Fig. 2). Importantly, user-defined phantoms are also supported, including, e.g., personalized phantoms derived from segmentations of data from tomographic anatomical imaging modalities (e.g. CT, MR) that have been converted to the standard tetrahedral *.ele/*.node format.

Specification of the calculation type, radionuclide, and simulation options (e.g. resolution, physical model options), is performed in the "Parameter Setting" module. Three general types of calculation can be configured: a) absorbed dose, b) dose rate, and c) computation of S-values to be used in outside calculations of mean region-level absorbed dose. Each output mode may be calculated at the tetrahedral region level or in 3D (voxel level). EGS5-mode(18) of PHITS is used for positron, negatron/electron, and photon transport; the default PHITS algorithm is utilized for alpha decay where applicable. The accuracy of EGS5-mode of PHITS in calculating dose-point kernels for mono-energetic electrons and beta-emitting isotopes was well-validated.(19) PARaDIM does not automatically account for decay of radionuclide progeny; i.e. the user must therefore ensure that if the radionuclide is part of a decay chain, the time-integrated activity coefficients for the progeny are characterized appropriately and simulated separately. Energy deposition arising from recoiling daughter nuclei is not scored.

Source particle generation for each phantom organ is conducted using the PHITS multi-source method; particle type is sampled based on weighted intensities defined by the PHITS radioisotope source libraries (equivalent to ICRP 107)(20), and the particle is given an initial energy sampled from the same libraries (full spectrum for betas and monoenergetic spectrum for photons/Auger/IC electrons/alpha). For radionuclides with multiple emission types, the user may specify which particle(s) to include in the simulation. Statistical uncertainties η for voxels or tetrahedral regions are calculated using “history variance mode” of PHITS, where the relative error is given as:

$$\eta = \frac{1}{\bar{X}} \sqrt{\frac{\sum_{i=1}^N (x_i w_i / \bar{w})^2 - N \bar{X}^2}{N(N-1)}} \quad \text{Eqn. 1}$$

where N is the total history number, x_i and w_i are tally results and the source weight of each sample, respectively, and \bar{X} and \bar{w} are the respective mean values of the tally results and source weights of N samples.

For the default absorbed dose calculation mode of PARaDIM, the source intensities are defined by whole-region time-integrated activity coefficients specified by the user within the ‘Source Definition’ module. For the dose rate calculation mode, input is given as either activities in source regions or fraction of administered activity in source regions. To configure an S-value calculation, one simply specifies the source region.

Several import/export and data processing options are provided to streamline workflow, and particularly for 3D mode, enable visualization and analysis (e.g. dose volume histogram generation) in numerous imaging softwares. Organ level absorbed doses output from PHITS are viewable in the PARaDIM graphical user interface for convenient readout.

PARaDIM was written entirely in Python (www.python.org); a description of libraries utilized in its development is provided in the Supplemental Information.

Example Dose Calculations in Human Phantoms

Dosimetric estimates for a ^{18}F -labeled reference PET tracer, $[^{18}\text{F}]\text{AIF-peptide}$, were obtained separately in PARaDIM and OLINDA 2.0 for the reference adult Korean man/woman using time-integrated activity coefficients extrapolated from mouse biodistribution data (see Table 2, and Supplemental Information). For these comparisons, male and female Mesh-type Reference Korean Phantoms(21) (MRKP-AM and MRKP-AF, respectively) were utilized in PARaDIM, whereas the adult male/female ICRP89(22) and legacy ORNL phantoms(23) were utilized in OLINDA with organ weights scaled to equivalent masses of the male/female MRKP. For organs in the MRKPs that are subdivided (e.g. the kidneys, comprised of separate tetrahedral regions defining the renal cortex, medulla, and pelvis as opposed to the entire kidneys) the time-integrated activity coefficient was allocated to each constituent component as the product of the component's mass fraction and the total time-integrated activity coefficient for the whole organ. One million total source particles were simulated in each phantom and PARaDIM defaults for all other parameters were utilized.

Organ-level mean absorbed doses for whole organs uniquely defined in the MRKP-AF/-AM phantoms (e.g. liver, brain) were output directly from PARaDIM/PHITS. To facilitate comparison of the results of PARaDIM with those of OLINDA 2.0, whole organ mean absorbed doses $D(r_{T:W}, T_D)$ for target organs that are subdivided into components $r_{T:C}$ of mass $m_{T:C}$, were calculated as:

$$D(r_{T:W}, T_D) = \frac{\sum_T D(r_{T:C}, T_D) \cdot m(r_{T:C})}{\sum_T m(r_{T:C})} \quad \text{Eqn. 3}$$

For further comparison and validation independent of the distribution of decays and geometry, the Supplemental Information provides S-values for selected sources/targets for ^{18}F in

the MRKP-AF/-AM phantoms which enables comparison of PARaDIM with other Monte Carlo transport codes.

Additionally, dose rates were calculated with PARaDIM in a phantom derived from segmentation of a PET/CT dataset (data obtained from the TCIA anti-PD-1_Melanoma collection)(24), demonstrating the use of patient-specific phantoms in PARaDIM. The parameters for this simulation were as described above.

Example Dose Calculation in Small-Animal Phantoms

The MOBY phantom has been implemented by several investigators for mouse dosimetry calculations (25–27). Using methodology described in the Supplemental Information, MOBY was converted to tetrahedral geometry to enable its use within PARaDIM; ^{18}F self S-values for MOBY's constituent organs were calculated and compared with previous literature which utilized voxel-based methods with this phantom. One million source particles were simulated separately from each organ, resulting in less than 1% relative uncertainty for each self S-value. Additionally, decay of ^{18}F , ^{90}Y and ^{186}Re , was simulated from MOBY liver sources in 3D mode (10^6 events, 0.75 mm resolution).

Example Cell-Level Dose Calculations

PARaDIM was compared with MIRDcell for validation of accuracy of absorbed dose computation at the cell level. MIRDcell models cells as concentric spheres, with radii of the cell nucleus and complete cell specified in integer increments of micrometers; the cell membrane, cytoplasm, nucleus, or entire cell may be utilized as sources or targets. Selected S-values for cells of various dimensions were generated with MIRDcell and compared with those computed

with PARaDIM using a series of tetrahedral cell phantoms constructed with equivalent dimensions (see Supplemental Information). One million source particles were simulated for ^{18}F and ^{211}At using PARaDIM's parameter defaults; calculations with MIRDcell utilized the full beta spectrum where applicable.

In contrast to MIRDcell, PARaDIM is not limited to cells modeled as concentric spheres with regular spacing. Within the constraints of computation time and memory, detailed arrays of cells with complicated geometry, arbitrary size, and non-uniform spacing may be defined as a tetrahedral mesh and utilized in dose calculations. As an illustration, a calculation for a hypothetical cell geometry similar to one encountered commonly in *in vitro* cell radioassays was designed. A “pellet” of 500 non-spheroidal cells contained in a 1.5 mL centrifuge vial in 370 μL of media was modeled as a tetrahedral mesh. 37 kBq of total ^{64}Cu activity was assumed to be distributed as follows: 9.5% within the cytoplasm of the cells, 0.5% within the cell nuclei, and 90% in the surrounding media.

RESULTS AND DISCUSSION

PARaDIM is a flexible tool for dosimetry in many settings relevant to nuclear medicine and radiation protection, yielding estimates of region-level and non-uniform absorbed doses using a tetrahedral mesh phantom to model the relevant anatomy/geometry. Whereas many softwares implement only one or a limited set of phantoms, a motivating factor for utilizing PARaDIM is the ability to easily simulate dose in novel phantoms. It is designed to integrate well with modern imaging software for output post-processing and visualization, and with workflows for development of bespoke phantoms, e.g., from segmentation of medical imaging data (Fig. 3). Figure 4 gives a cell-based example that is necessarily situational, but further illustrates PARaDIM's utility for dose calculation in truly unique/customized settings, especially when allied

with computer-aided design workflows for custom phantom generation (we note this is facilitated by PARaDIM's use of tetrahedral mesh phantoms). Other use-cases where PARaDIM excels include advanced phantoms where complex source and target regions are detailed, computational reference phantoms for which S-values have not yet been calculated, as well as reference phantoms which have been deformed (e.g., to match a particular subject's geometry). PARaDIM is also capable for dose calculation in brachytherapy and certain external radionuclide exposure scenarios. Such calculations can be accomplished e.g. by defining brachytherapy/external sources along with the biological system together, within a single tetrahedral mesh (Supplemental Fig. 2); however, validation of the program for these purposes is outside the scope of the present manuscript. Finally, 4D dose calculations may be conducted in PARaDIM by importing a dynamic geometry as separate static "frames".

Agreement of PARaDIM with Other Methods

We have compared absorbed doses computed with PARaDIM to two widely used and well-validated applications for internal dosimetry: OLINDA 2.0 and MIRDcell. While the validation presented is not exhaustive, the agreement provides some confidence in PARaDIM's results and illustrates the value of PARaDIM as both a stand-alone dosimetry tool and as a complement to these well-established methods. Human organ-level absorbed doses calculated with PARaDIM and OLINDA agreed well, within ~20% for most organs, with differences attributed primarily to geometric and spatial differences between the MRKP-AF/-AM phantoms used in PARaDIM, and the ICRP89 series/stylized ORNL reference human phantoms utilized in the latter program (Fig. 5). The most significant differences observed were for organs comprised of separate "wall" and "contents" components (e.g. urinary bladder wall, heart wall) where doses computed with OLINDA were higher than PARaDIM – these differences were not unexpected, as OLINDA calculates

doses to the “wall” target regions r_T from “contents” sources r_s by assuming the specific absorbed fraction $\Phi(r_T \leftarrow r_s)$ for beta radiations is approximately given by the following(28):

$$\Phi(r_T \leftarrow r_s) = 1/2 \cdot M(r_s) \quad \text{Eqn. 4}$$

which is known to yield conservatively high estimates for low energy beta emitters including ^{18}F . The corresponding 3D output of PARaDIM for these simulations is shown in Figure 6.

Self S-values for the MOBY mouse phantom showed good agreement with previous work(25) (Table 3); overall agreement was within 10% for all organs, but the S-values computed with PARaDIM showed a positive bias of approximately 4% on average, expected to be due in part to differences in algorithm (GEANT4 vs. PHITS-EGS5) as well as due to geometric and partial volume considerations arising from the use of voxel vs. tetrahedral mesh methods. The agreement with MIRDcell for cellular S-value calculations was similarly good (< 10%) for both high-LET and low-LET emitters, with the largest differences arising for the nucleus self-S (i.e. $S(N \leftarrow N)$) (Table 4). The reason for this difference is expected to be due primarily to difference in the algorithms and cross-sectional data utilized, where MIRDcell utilizes an analytical method based on stopping power and geometrical factors(29), in contrast to PARaDIM’s use of PHITS.

Computational Speed

Computation times in PARaDIM are variable – influenced heavily by the particle history number, the level of detail of the phantom, spatial dimensions of the phantom, selected output resolution, decay modes and energies of the radionuclide simulated, energy cutoffs, and the computer hardware and architecture used. Generally, PARaDIM does not require supercomputing clusters or other expensive computational assets for most simulations. By default, calculations are run on a single core, but both shared-memory parallel processing and

manual parallel processing are supported for acceleration. For reference, the MRKP-AF/-AM simulations described in herein required 3-4 hours of computation time for a single-core calculation on a standard desktop workstation (3.6 GHz Intel Xeon 5122 processor, Windows 10 OS). In contrast, the computation time for the cell S-value calculations given the same particle history number (10^6), was generally less than 5 min, owing to the reduced size and complexity of the cell phantoms utilized.

Advantages and Disadvantages of the Multi-Source Technique Relative to the S-value Approach

While dosimetry calculations based on pre-computed S-values produces essentially instantaneous results, in any novel phantom, the S-values must be first determined. Relative to the *en masse* multi-source technique that PARaDIM is capable of utilizing, calculation of S-values for each individual tissue in a phantom, to the same degree of relative uncertainty, is computationally intensive and requires a vast amount of oversampling if the source distribution is unknown. The reason for this arises because, for most tissues, the absorbed dose contribution from decays occurring in distant sources or sources with a low density of decays, is generally dominated by that from one or two “hot” sources, and/or that imparted from decays occurring within or adjacent to the target. Furthermore, in the *en masse* method of calculation, sampling statistics are necessarily increased in regions with elevated dose, where accuracy is often more important; in this respect, however, attention must be paid to the individual tissue radiation weighting factors. PARaDIM does not incorporate such radiation weighting factors (i.e. only absorbed dose is scored, not dose equivalent), but if needed, weighting factors may be applied to the output in other standard software (e.g. MS Excel).

Evaluation of Non-Uniform Dose Deposition with PARaDIM

Non-uniform dose deposition arising from sources with homogeneous distributions of radioactivity may be evaluated in 3D mode within structures that can be sufficiently resolved at the specified voxel size, and for radiations with a penetration range that is long in comparison to the voxel size. As an example, absorbed dose from MOBY phantom liver sources was calculated in 3D mode (with 0.75 mm isotropic voxel dimensions) using three radionuclides with largely different mean beta emission energies (Fig. 7). The mean soft tissue range of beta radiations emitted from ^{18}F and ^{186}Re are only 0.6 mm and 1.0mm, respectively. As these ranges are not long in comparison to the voxel size, in this case this resolution is largely unsuitable for evaluating variation in deposited dose due to beta emissions from either ^{18}F or ^{186}Re due to partial volume effects. Dose-volume histograms were derived from the 3D dose distributions to help illustrate this point; differences in the respective normalized dose-volume histograms for ^{18}F and ^{186}Re (Fig. 7C) are not meaningfully different, despite the large relative difference in mean beta energy/range between these radionuclides. Conversely, the mean range of beta emissions from ^{90}Y is 3.9 mm, which is large relative to the voxel dimensions, and the variation in dose within the liver and dose to organs surrounding the liver could be meaningfully assessed by defining regions/volumes of interest, or globally within organs using a dose-volume histogram. Similarly, 511 keV photons produced by ^{18}F positron annihilation are very long range in this respect, and the variation in dose deposition at sites distant from the liver, is evident (Fig. 7A); this effect is absent from the ^{186}Re and ^{90}Y simulations due to their low abundance of energetic photons.

Alternatively, non-uniform doses within phantom regions may be evaluated to increased extents by subdividing regions into sub-regions using mesh editing software; the mean dose within each sub-region would then be tallied individually in PARaDIM. This approach avoids the partial volume effects associated with voxel-format dose tallies.

CONCLUSION

Advancements in medical image segmentation, 3D geometric modeling/manipulation/representation/visualization, and Monte Carlo particle transport simulation have enabled the accurate calculation of absorbed doses in tetrahedral mesh phantoms that intricately characterize the anatomy of subjects including humans, animals, and cells. The utilization of such phantoms in dosimetric simulations has previously been largely restricted to those with an advanced understanding of select Monte Carlo transport codes. PARaDIM extends the benefits of this powerful simulation technique to all investigators in the field without the need for advanced computer expertise, and can be obtained freely at [<url>](#) along with its terms of use, disclaimer, and documentation.

ACKNOWLEDGEMENTS AND DISCLOSURES

The authors gratefully acknowledge the Memorial Sloan Kettering Radiochemistry and Molecular Imaging Probes core, which was supported in part by NIH grant P30 CA08748. We gratefully acknowledge Mr. William H. and Mrs. Alice Goodwin and the Commonwealth Foundation for Cancer Research and The Center for Experimental Therapeutics of Memorial Sloan Kettering Cancer Center (JSL). LMC acknowledges support from the Ruth L. Kirschstein NRSA Postdoctoral Fellowship (NIH F32 EB025050). No potential conflict of interest relevant to this article was reported.

KEY POINTS

Question

Can we facilitate the use of advanced methods in Monte Carlo-based internal dosimetry by scientists and clinicians?

Pertinent Findings

PARaDIM, a user-friendly graphical user interface for internal dose calculations via PHITS was developed, tested, and validated in this work.

Implications for Basic Science and Patient Care

PARaDIM will benefit the field by facilitating setup of internal dose calculations with modern computational reference phantoms and subject-specific phantoms derived from anatomical imaging, offering an advanced alternative to existing methods for radiation dose assessment.

REFERENCES

1. Stabin MG, Sparks RB, Crowe E. OLINDA/EXM: The second-generation personal computer software for internal dose assessment in nuclear medicine. *J Nucl Med*. 2005;46:1023-1027.
2. Kost SD, Dewaraja YK, Abramson RG, Stabin MG. VIDA: A voxel-based dosimetry method for targeted radionuclide therapy using Geant4. *Cancer Biother Radiopharm*. 2015;30:16-26.
3. Bednarz B, Grudzinski J, Marsh I, et al. Murine-specific internal dosimetry for preclinical investigations of imaging and therapeutic agents. *Health Phys*. 2018;114:450-459.
4. Sgouros G, Frey E, Wahl R, He B, Prideaux A, Hobbs R. Three-dimensional imaging-based radiobiological dosimetry. *Semin Nucl Med*. 2008;38:321-334.
5. Prideaux AR, Song H, Hobbs RF, et al. Three-dimensional radiobiologic dosimetry: application of radiobiologic modeling to patient-specific 3-dimensional imaging-based internal dosimetry. *J Nucl Med*. 2007;48:1008-1016.
6. Goddu SM, Rao DV, Howell RW. Multicellular dosimetry for micrometastases: dependence of self-dose versus cross-dose to cell nuclei on type and energy of radiation and subcellular distribution of radionuclides. *J Nucl Med*. 1994;35:521-530.
7. Makrigiorgos GM, Adelstein SJ, Kassis AI. Limitations of conventional internal dosimetry at the cellular level. *J Nucl Med*. 1989;30:1856-1864.
8. Vaziri B, Wu H, Dhawan AP, et al. MIRD Pamphlet No. 25: MIRDcell V2.0 software tool for dosimetric analysis of biologic response of multicellular populations. *J Nucl Med*. 2014;55:1557-1564.
9. Sato T, Iwamoto Y, Hashimoto S, et al. Features of Particle and Heavy Ion Transport code System (PHITS) version 3.02. *J Nucl Sci Tech*. 2018;55:684-690.
10. Iwamoto Y, Sato T, Hashimoto S, et al. Benchmark study of the recent version of the PHITS code. *J Nucl Sci Tech*. 2017;54:617-635.
11. Bolch WE, Eckerman KF, Sgouros G, Thomas SR. MIRD pamphlet No. 21: a generalized schema for radiopharmaceutical dosimetry--standardization of nomenclature. *J Nucl Med*. 2009;50:477-484.
12. Furuta T, Sato T, Han MC, et al. Implementation of tetrahedral-mesh geometry in Monte Carlo radiation transport code PHITS. *Phys Med Biol*. 2017;62:4798.
13. Yeom YS, Jeong JH, Han MC, Kim CH. Tetrahedral-mesh-based computational human phantom for fast Monte Carlo dose calculations. *Phys Med Biol*. 2014;59:3173-3185.
14. Kim CH, Yeom YS, Nguyen TT, et al. The reference phantoms: voxel vs polygon
,
The reference phantoms: voxel vs polygon. *Ann ICRP*. 2016;45:188-201.

15. Choi C, Nguyen TT, Yeom YS, et al. Mesh-type reference Korean phantoms (MRKPs) for adult male and female for use in radiation protection dosimetry. *Phys Med Biol.* 2019;8:64.
16. Yeom YS, Han MC, Choi C, et al. Computation Speeds and Memory Requirements of Mesh-Type ICRP Reference Computational Phantoms in Geant4, MCNP6, and PHITS. *Health Phys.* 2019;116:664-676.
17. Lee H, Yeom YS, Nguyen TT, et al. Percentile-specific computational phantoms constructed from ICRP mesh-type reference computational phantoms (MRCPs). *Phys Med Biol.* 2019;64:045005.
18. Hirayama H, Namito Y, Bielajew AF, Wilderman SJ, Nelson WR. The EGS5 code system. High Energy Accelerator Research Organization; 2005.
19. Shiiba T, Kuga N, Kuroiwa Y, Sato T. Evaluation of the accuracy of mono-energetic electron and beta-emitting isotope dose-point kernels using particle and heavy ion transport code system: PHITS. *Appl Radiat Isot.* 2017;128:199-203.
20. Eckerman K, Endo A. ICRP Publication 107. Nuclear decay data for dosimetric calculations. *Ann ICRP.* 2008;38:7-96.
21. Choi C, Nguyen TT, Yeom YS, et al. Mesh-type reference Korean phantoms (MRKPs) for adult male and female for use in radiation protection dosimetry. *Phys Med Biol.* 2019;64:085020.
22. Valentin J. Basic anatomical and physiological data for use in radiological protection: reference values: ICRP Publication 89. *Ann ICRP.* 2002;32:1-277.
23. Cristy M, Eckerman KF. Specific absorbed fractions of energy at various ages from internal photon sources: 7, Adult male. Oak Ridge National Lab.; 1987.
24. Clark K, Vendt B, Smith K, et al. The Cancer Imaging Archive (TCIA): maintaining and operating a public information repository. *J Digit Imaging.* 2013;26:1045-1057.
25. Keenan MA, Stabin MG, Segars WP, Fernald MJ. RADAR realistic animal model series for dose assessment. *J Nucl Med.* 2010;51:471-476.
26. Kostou T, Papadimitroulas P, Loudos G, Kagadis GC. A preclinical simulated dataset of S - values and investigation of the impact of rescaled organ masses using the MOBY phantom. *Phys Med Biol.* 2016;61:2333-2355.
27. Larsson E, Ljungberg M, Strand S-E, Jönsson B-A. Monte Carlo calculations of absorbed doses in tumours using a modified MOBY mouse phantom for pre-clinical dosimetry studies. *Acta Oncologica.* 2011;50:973-980.
28. Stabin M, Siegel J. Physical models and dose factors for use in internal dose assessment. *Health Phys.* 2003;85:294-310.
29. Goddu SM, Howell RW, Rao DV. Cellular dosimetry: absorbed fractions for monoenergetic electron and alpha particle sources and S-values for radionuclides uniformly distributed in different cell compartments. *J Nucl Med.* 1994;35:303-316.

30. Dogdas B, Stout D, Chatziioannou AF, Leahy RM. Digimouse: a 3D whole body mouse atlas from CT and cryosection data. *Phys Med Biol.* 2007;52:577-587.

FIGURES AND TABLES

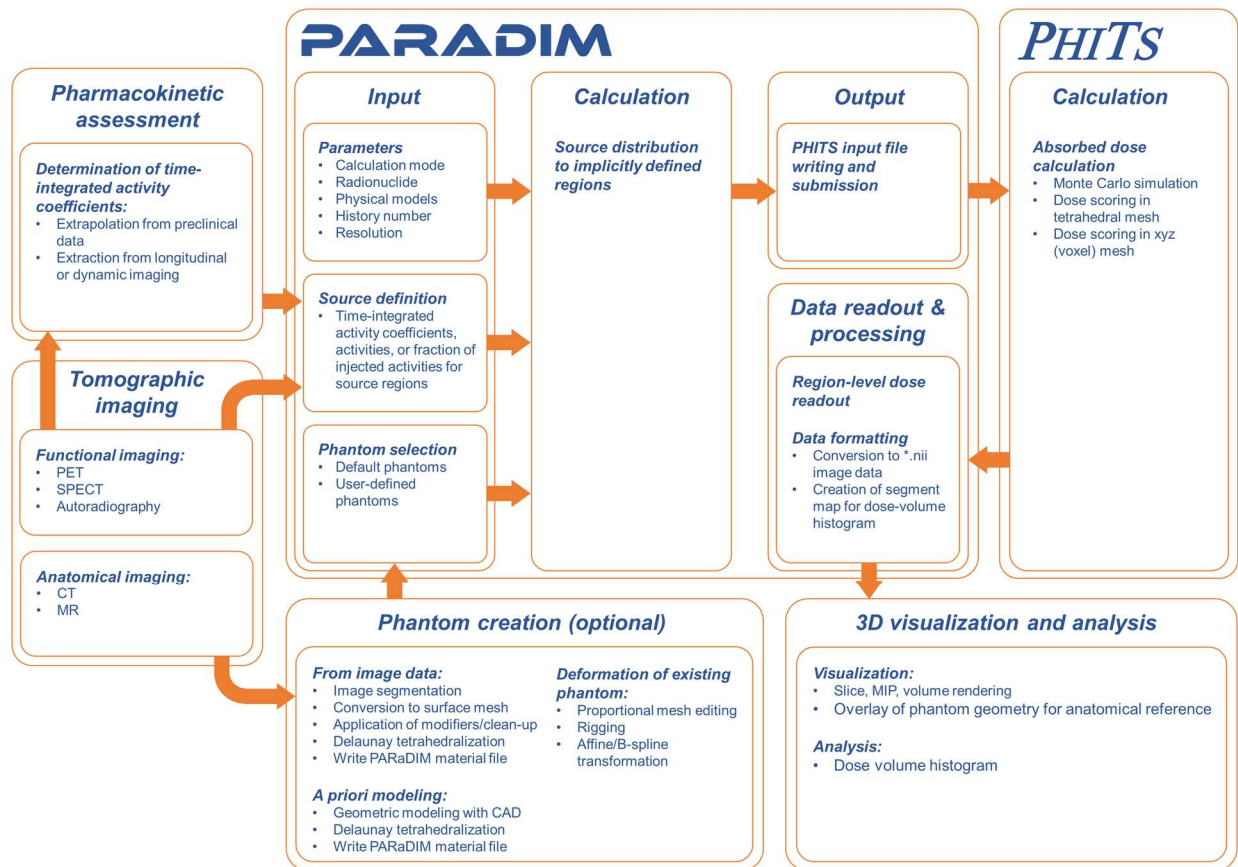


Figure 1: Flowchart describing the function of PARaDIM for organ-level and 3D dose calculation and relationships with relevant techniques.

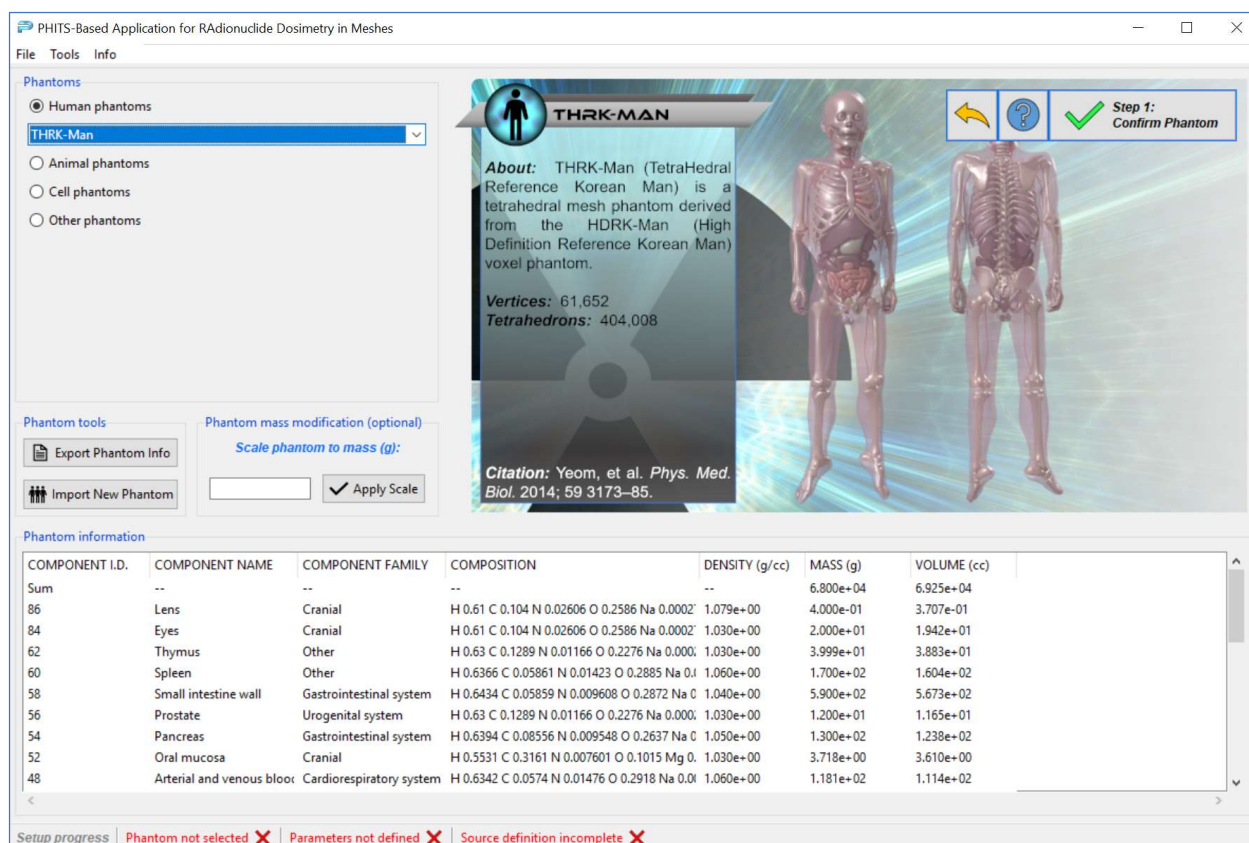


Figure 2: Snapshot of the “Phantom Selection” module in PARaDIM. Here the user may select a phantom from the library, or may add a phantom to the standard library via the “Add New Phantom” function. Tissues and masses for the currently selected phantom may be viewed or exported. Phantoms may be scaled to a particular mass by providing an entry in the “Scale to mass” input field.

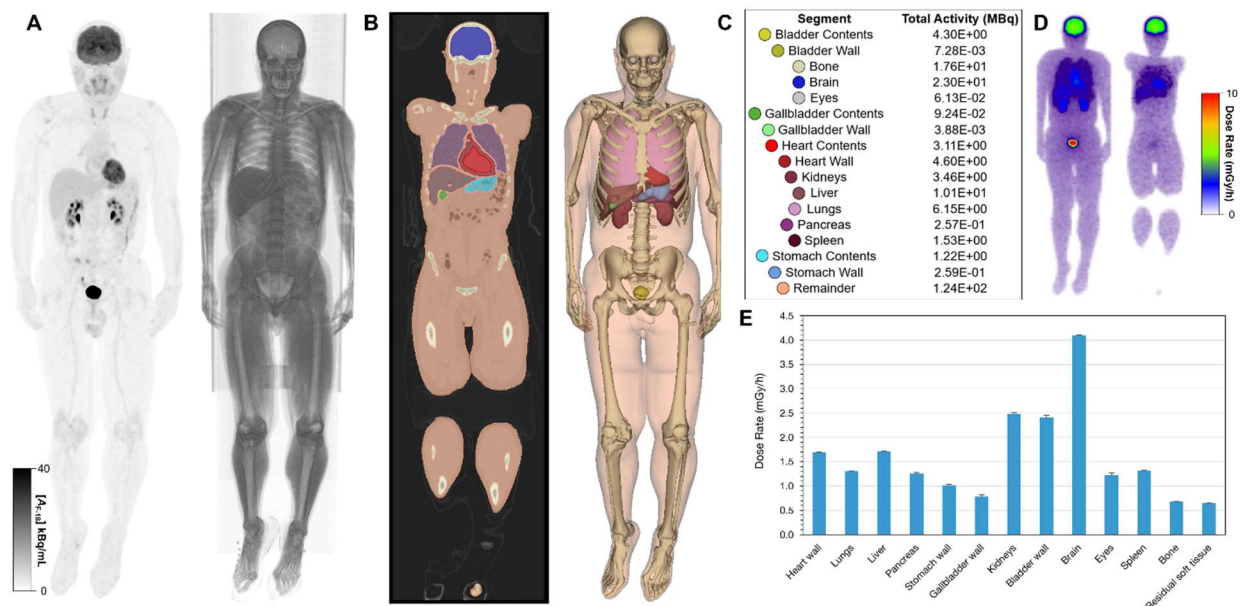


Figure 3: Conceptual example of patient-specific, tomographic imaging-derived phantom utilization in PARaDIM; quantification of dose rate at scan time during re-staging with [^{18}F]-FDG. A) [^{18}F]-FDG PET maximum-intensity projection and volume-rendered CT. B) Slice and 3D-rendered view of CT-based segmentation. C) Quantification of ^{18}F activity in the co-registered PET volume within each segment. D) Maximum intensity projection and slice view of 3D output following dose rate simulation in PARaDIM (1×10^6 events simulated). E) Mean organ-level dose rate output from PARaDIM.

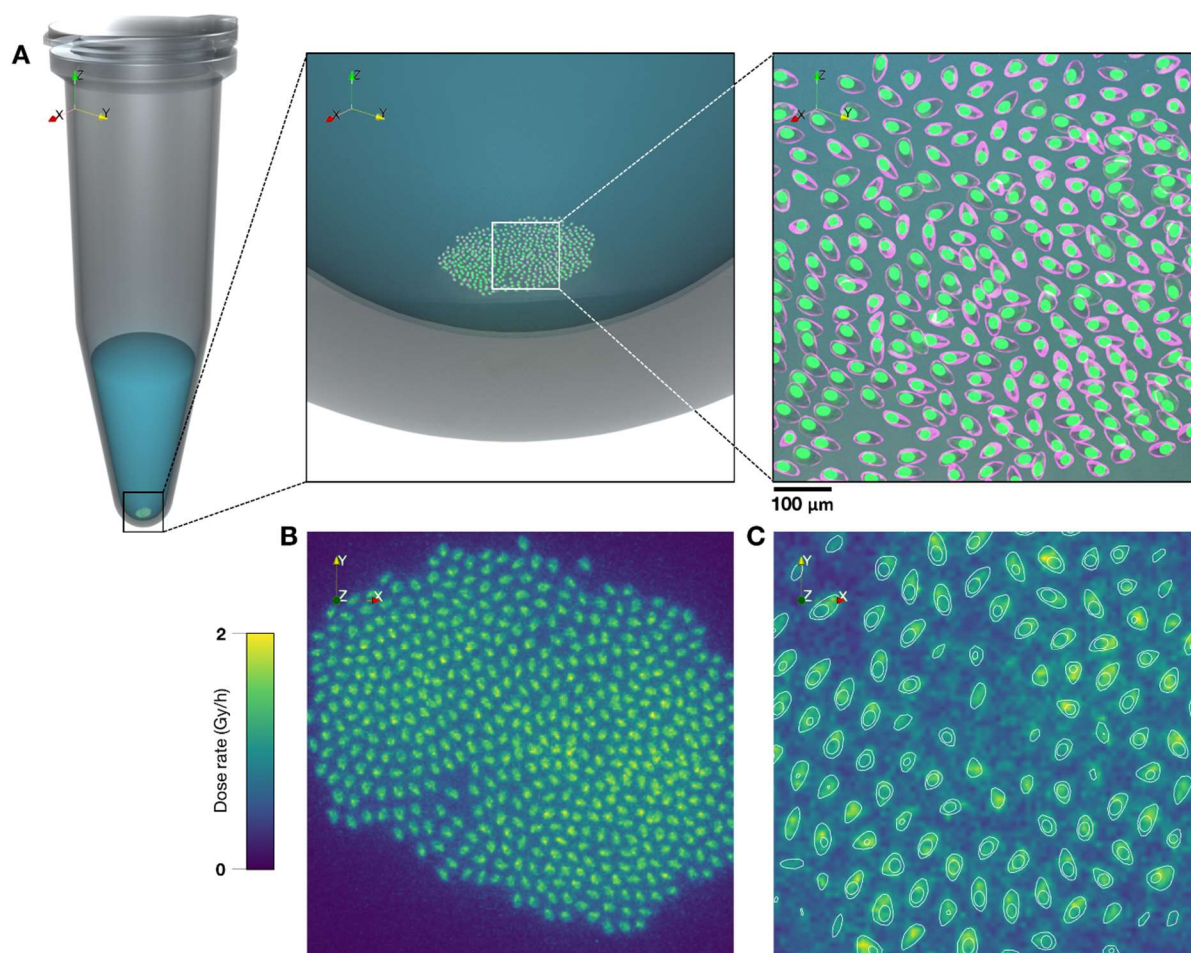


Figure 4: Cell-level dose rate calculation for a step of an *in vitro* radioassay. A) 3D rendering of the system. B,C) Dose rate scored at voxel level for the cell array (6 μm isotropic voxel size, 1×10^7 total history number): maximum intensity projection (B) and slice view with cell boundary overlay (C).

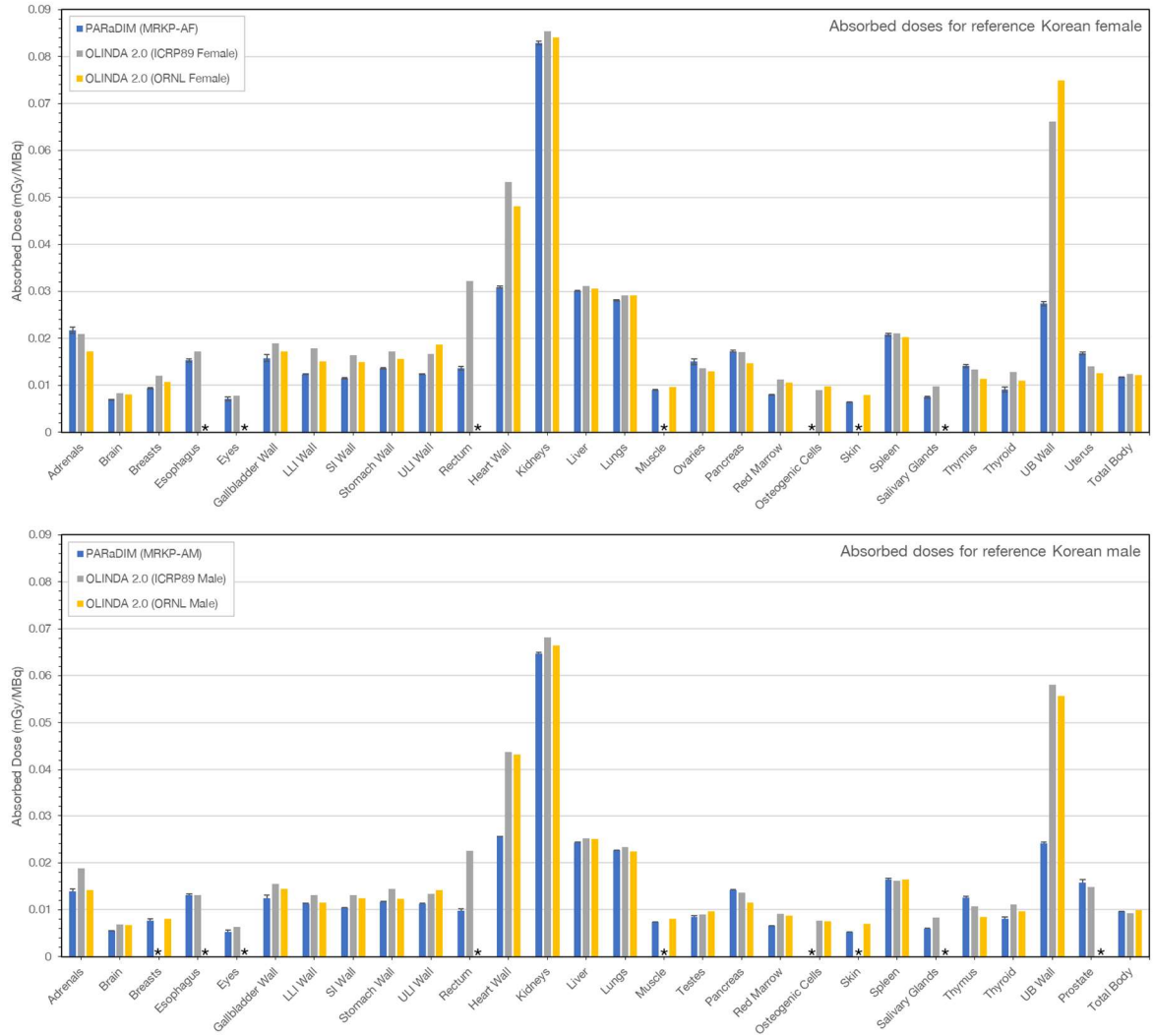


Figure 5: Absorbed dose estimation for I.V. administration of $[^{18}\text{F}]\text{AIF-peptide}$ in reference Koreans. Comparison of organ-level doses computed with PARaDIM vs. OLINDA 2.0 for males (top) and females (bottom). Asterisks represent tissues not defined in the respective phantom.

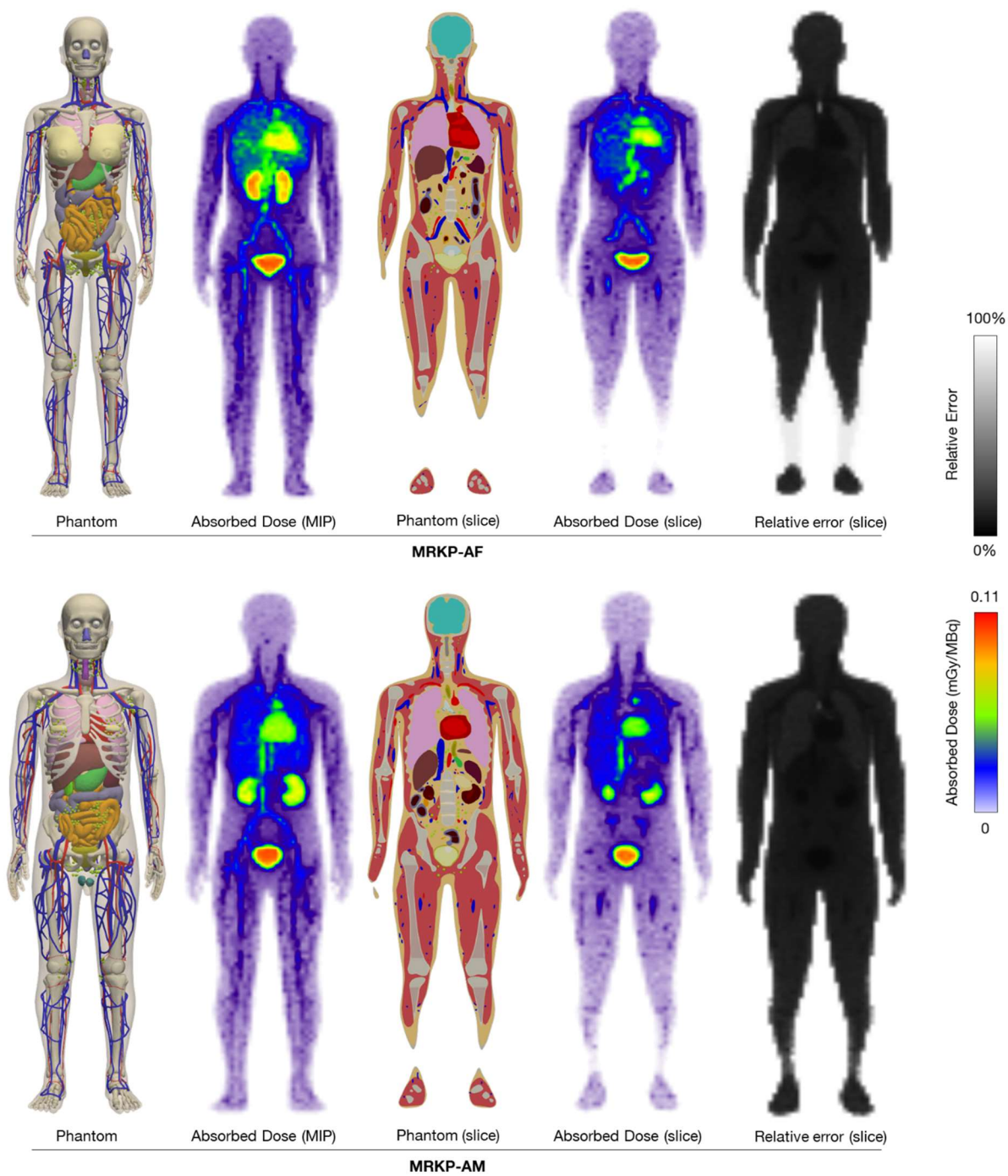


Figure 6: Absorbed doses and corresponding relative uncertainties scored at the voxel level in the MRKP-AM and MRKP-AF phantoms, with phantom geometry juxtaposed for anatomical reference.

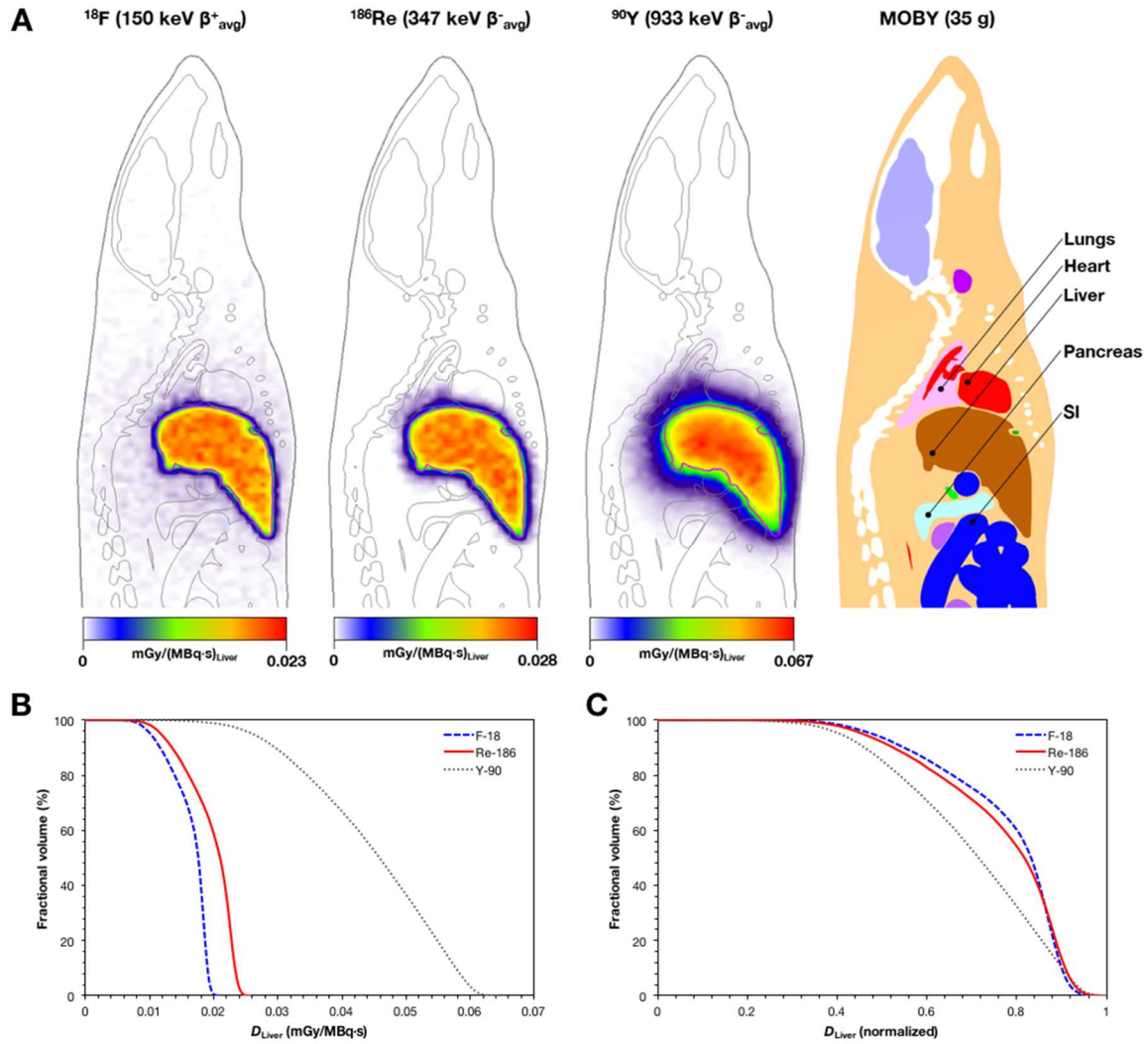


Figure 7: Evaluation of inhomogeneous dose deposition in MOBY phantom with PARaDIM. A) Radionuclides with increasingly energetic beta emissions simulated from liver sources. Note the shallow gradient of dose deposition at the liver boundaries (magenta outline) and significant dose to adjacent organs with ^{90}Y , in comparison to shorter-range beta emitters ^{18}F and ^{186}Re . B) Dose-volume histograms for the liver, for each radionuclide. C) Dose volume histograms from (B) normalized to the maximum-dose voxel.

Table 1: Pre-configured tetrahedral phantoms available for PARaDIM.

Phantom	Type	Size (MB)	Description
MRCP series*	Human	~380	Collection of 9 female and 9 male percentile-specific reference phantoms(17)
MRKP series*	Human	~380	Set of reference Korean phantoms (male/female)(21)
THRK-Man*	Human	~20	Reference Korean man for accelerated simulations
Digimouse	Mouse		Original Digimouse tessellated atlas(30)
Digimouse-HR series†	Mouse	~67	High-resolution series of Digimouse phantom
SC10 series†	Cell	~1	Collection of concentric spherical cell phantoms of 10um outer diameters and various nuclear diameters; scalable for modeling larger/smaller cells
Unit-mass sphere†	Geometric primitive	~0.5	Unit-mass icosphere (4 subdivisions), scalable for modeling tumors or for benchmark calculations

*Denotes phantom requiring license agreement

†Denotes phantom created or modified in this work

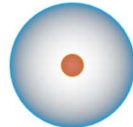
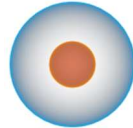
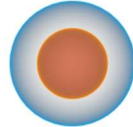
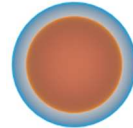
Table 2: Time-integrated activity coefficients used for absorbed dose calculations in PARaDIM and OLINDA 2.0, calculated for reference Korean man/woman based on mouse biodistribution of reference peptide.

Organ	Time-integrated activity coefficient (MBq*h/MBq)	
	Male	Female
Left colon contents	0.00283	0.00281
Small Intestine contents	0.00743	0.0073
Stomach Contents	0.00443	0.00423
Right colon contents	0.00283	0.00281
Heart contents	0.111	0.103
Heart wall	0.025	0.028
Kidneys	0.111	0.124
Liver	0.119	0.13
Lungs	0.121	0.116
Pancreas	0.00309	0.0034
Spleen	0.00812	0.00949
Urinary bladder contents	0.0954	0.0954
Remainder	1.53	1.51

Table 3: S-values for ^{18}F in the MOBY phantom in comparison to those reported by Keenan et al.(25)
Differences are reported relative to the values of (25).

MOBY Organ	Mass (g)	Self-S (mGy/MBq*s) Keenan et al.(25)	Self-S (mGy/MBq*s) PARaDIM	% Difference
Brain	0.568	6.71E-02	6.63E-02	1.23
Heart	0.291	1.27E-01	1.14E-01	9.89
Kidneys	0.374	9.68E-02	9.59E-02	0.94
Liver	2.15	1.82E-02	1.77E-02	2.55
Lungs	0.107	2.14E-01	2.08E-01	2.88
Pancreas	0.378	9.15E-02	8.88E-02	2.98
Skeleton	2.61	1.23E-02	1.14E-02	7.52
Spleen	0.136	2.56E-01	2.49E-01	2.55
Testes	0.197	1.81E-01	1.73E-01	4.24
Thyroid	0.016	1.93E+00	1.86E+00	3.63
Bladder	0.075	4.59E-01	4.52E-01	1.54
Total body	29.8	1.54E-03	1.46E-03	5.30

Table 4: S-values for ^{18}F (positron, 250 keV_{avg}) and ^{211}At (alpha, 5.87 MeV_{avg}) in spherical cells computed with PARaDIM in comparison with MIRDcell. Differences are reported relative to MIRDcell.

Cell Dimensions	$S(r_T \leftarrow r_s)$	Radionuclide	PARaDIM (Gy/Bq·s)	MIRDcell (Gy/Bq·s)	% Difference
$R_C = 5\ \mu\text{m}, R_N = 1\ \mu\text{m}$ 	$S(N \leftarrow CS)$	^{18}F	$1.547\text{E-}04 \pm 1.90\%$	$1.58\text{E-}04$	2.12%
		^{211}At	$1.895\text{E-}02 \pm 1.70\%$	$1.78\text{E-}02$	-7.57%
	$S(C \leftarrow CS)$	^{18}F	$2.306\text{E-}04 \pm 0.08\%$	$2.35\text{E-}04$	1.87%
		^{211}At	$2.832\text{E-}02 \pm 0.17\%$	$2.66\text{E-}02$	-4.93%
	$S(N \leftarrow Cy)$	^{18}F	$4.010\text{E-}04 \pm 1.20\%$	$4.00\text{E-}04$	-0.24%
		^{211}At	$4.656\text{E-}02 \pm 1.60\%$	$4.48\text{E-}02$	-3.52%
	$S(C \leftarrow C)$	^{18}F	$3.434\text{E-}04 \pm 0.16\%$	$3.51\text{E-}04$	2.17%
		^{211}At	$4.189\text{E-}02 \pm 0.28\%$	$3.99\text{E-}02$	-4.91%
$R_C = 5\ \mu\text{m}, R_N = 2\ \mu\text{m}$ 	$S(N \leftarrow CS)$	^{18}F	$1.644\text{E-}04 \pm 0.22\%$	$1.62\text{E-}04$	-1.45%
		^{211}At	$1.976\text{E-}02 \pm 0.94\%$	$1.83\text{E-}02$	-8.00%
	$S(C \leftarrow CS)$	^{18}F	$2.310\text{E-}04 \pm 0.62\%$	$2.35\text{E-}04$	1.68%
		^{211}At	$2.791\text{E-}02 \pm 0.51\%$	$2.66\text{E-}02$	-4.91%
	$S(N \leftarrow Cy)$	^{18}F	$3.337\text{E-}04 \pm 0.16\%$	$3.36\text{E-}04$	0.69%
		^{211}At	$3.872\text{E-}02 \pm 0.67\%$	$3.76\text{E-}02$	-2.98%
	$S(C \leftarrow C)$	^{18}F	$3.424\text{E-}04 \pm 0.84\%$	$3.51\text{E-}04$	2.46%
		^{211}At	$4.157\text{E-}02 \pm 0.61\%$	$3.99\text{E-}02$	-4.18%
$R_C = 5\ \mu\text{m}, R_N = 3\ \mu\text{m}$ 	$S(N \leftarrow CS)$	^{18}F	$1.719\text{E-}04 \pm 0.64\%$	$1.71\text{E-}04$	-0.53%
		^{211}At	$1.934\text{E-}02 \pm 0.53\%$	$1.92\text{E-}02$	-0.75%
	$S(C \leftarrow CS)$	^{18}F	$2.309\text{E-}04 \pm 0.16\%$	$2.35\text{E-}04$	1.73%
		^{211}At	$2.754\text{E-}02 \pm 0.52\%$	$2.66\text{E-}02$	-3.53%
	$S(N \leftarrow Cy)$	^{18}F	$2.828\text{E-}04 \pm 0.99\%$	$2.85\text{E-}04$	0.78%
		^{211}At	$3.872\text{E-}02 \pm 0.67\%$	$3.76\text{E-}02$	-2.98%
	$S(C \leftarrow C)$	^{18}F	$3.422\text{E-}04 \pm 0.27\%$	$3.51\text{E-}04$	2.50%
		^{211}At	$4.166\text{E-}02 \pm 0.50\%$	$3.99\text{E-}02$	-4.41%
$R_C = 5\ \mu\text{m}, R_N = 4\ \mu\text{m}$ 	$S(N \leftarrow CS)$	^{18}F	$1.857\text{E-}04 \pm 0.66\%$	$1.86\text{E-}04$	0.16%
		^{211}At	$2.134\text{E-}02 \pm 0.55\%$	$2.10\text{E-}02$	-1.64%
	$S(C \leftarrow CS)$	^{18}F	$2.309\text{E-}04 \pm 0.28\%$	$2.35\text{E-}04$	1.75%
		^{211}At	$2.763\text{E-}02 \pm 0.42\%$	$2.66\text{E-}02$	-3.89%
	$S(N \leftarrow Cy)$	^{18}F	$2.451\text{E-}04 \pm 0.87\%$	$2.48\text{E-}04$	1.18%
		^{211}At	$2.881\text{E-}02 \pm 0.65\%$	$2.79\text{E-}02$	-3.27%
	$S(C \leftarrow C)$	^{18}F	$3.422\text{E-}04 \pm 0.58\%$	$3.51\text{E-}04$	2.50%
		^{211}At	$4.130\text{E-}02 \pm 0.46\%$	$3.99\text{E-}02$	-3.52%
$S(N \leftarrow N)$	^{18}F	$5.314\text{E-}04 \pm 1.10\%$	$5.67\text{E-}04$	6.28%	
	^{211}At	$6.609\text{E-}02 \pm 0.59\%$	$6.44\text{E-}02$	-2.62%	

SUPPLEMENTARY INFORMATION FOR:

PARaDIM – A PHITS-based Monte Carlo tool for internal dosimetry with tetrahedral mesh computational phantoms

Lukas M. Carter^{*1}, Troy M. Crawford^{*2}, Tatsuhiko Sato^{3,4}, Takuya Furuta³, Chansoo Choi⁵, Chan Hyeon Kim⁵, Justin L. Brown⁶, Wesley E. Bolch⁶, Pat B. Zanzonico⁷, Jason S. Lewis^{1,8}

Affiliations:

¹Department of Radiology, Program in Pharmacology and the Radiochemistry and Molecular Imaging Probes Core, Memorial Sloan Kettering Cancer Center, New York, NY, USA

²Department of Physics, University of Rhode Island, Kingston, RI, USA

³Japan Atomic Energy Agency, Ibaraki, Japan

⁴Research Center for Nuclear Physics, Osaka University, Osaka, Japan

⁵Department of Nuclear Engineering, Hanyang University, Seoul, Korea

⁶J. Crayton Pruitt Family Department of Biomedical Engineering, University of Florida, Gainesville, FL, USA

⁷Department of Medical Physics, Memorial Sloan Kettering Cancer Center, New York, NY, USA

⁸Department of Radiology and Department of Pharmacology, Weill Cornell Medical College, New York, NY, USA

*Authors contributed equally to the manuscript

PARaDIM code development

PARaDIM is provided as a standalone executable for Windows operating systems. The source code was entirely written in Python (www.python.org) within the PyCharm integrated-development environment (<https://www.jetbrains.com/pycharm/>). The graphical user interface was created using the built-in Tkinter and Tk libraries, and the external libraries Numpy(1) and NiBabel(2) are utilized for select data processing functions. The code was interpreted with Python 3.6 and compiled using PyInstaller (www.pyinstaller.org). Each portion of the code was tested with PHITS versions 3.07-3.10 on Windows 7 and Windows 10 platforms, as the code was developed.

Estimation of human whole-organ time-integrated activity coefficients from mouse biodistribution data

All animal experiments were conducted in accordance with the guidelines approved by the Research Animal Resource Center (RARC) and Institutional Animal Care and Use Committee (IACUC) at Memorial Sloan Kettering Cancer Center.

For specification of the quantity of nuclear transformations occurring in source organs, PARaDIM utilizes the Medical Internal Radiation Dose Committee (MIRD) concept of the time-integrated activity coefficient $\tilde{a}(r_s, T_D)$, formerly known as the residence time(3):

$$\tilde{a}(r_s, T_D) = \frac{1}{A_0} \int_0^{T_D} A(r_s, t) dt \quad \text{Eqn. 1}$$

where A_0 is the initial administered activity, t is the time post-administration of the radiopharmaceutical, $A(r_s, t)$ is the time-dependent activity in source organ r_s , and T_D is the dose integration period (commonly taken as 0 (i.e. the time of administration) to ∞). The time-integrated activity coefficient for a given source organ thus represents the total number of decays of a radionuclide occurring in that organ, over a particular time integration interval, normalized to the administered activity. In PARaDIM, the time-integrated activity coefficient may be expressed in any matching activity units, but the time unit must be expressed in hours (e.g. $\mu\text{Ci}\cdot\text{h}/\mu\text{Ci}$, $\text{MBq}\cdot\text{h}/\text{MBq}$, etc.).

Whole organ time-integrated activity coefficients for a ^{18}F -labeled reference PET tracer, $[^{18}\text{F}]\text{AIF-peptide}$, were estimated for the reference adult Korean man/woman (using the MRKP-AF/MRKP-AM phantoms, respectively) by extrapolation of *ex vivo* biodistribution data for this tracer obtained in healthy C57BL/6 mice. Five cohorts of four mice each (20 mice in total) were injected with $[^{18}\text{F}]\text{AIF-peptide}$ ($\approx 20\mu\text{Ci}$, $1\mu\text{g}$, $200\mu\text{L}$) via the lateral tail vein. The activity in each syringe was measured both pre- and post-injection for accurate estimation of the administered activity. Mice were sacrificed via CO_2 asphyxiation at 0.5, 1, 2, 4, and 6h post-injection, and major organs harvested and weighed for *ex vivo* gamma counting. Organs were counted for 1min, resulting in less than 10% counting error for each measurement. Net count rates were converted to activities using a counter calibration factor and organ activity concentrations were expressed in percent of injected dose per gram of tissue (%ID/g) were calculated, decay-corrected to the time of injection (Fig. 1).

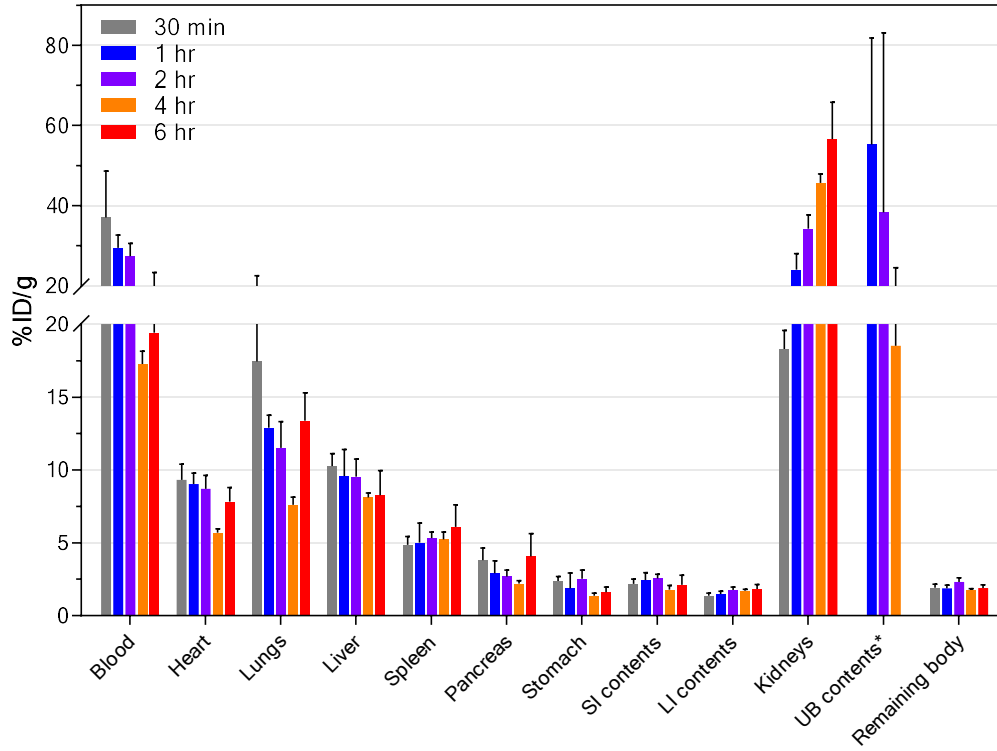


Fig. 1: Ex vivo mouse biodistribution data of an ^{18}F -labeled reference peptide, quantified in percentage injected dose per gram (%ID/g) corrected for decay back to time of injection.

The organ uptake values were converted to standardized uptake values (SUVs) for estimation of human organ absorbed doses. The percentage of injected dose in human organ I , $\%ID_I$, was obtained from Eqn. 1, which assumes SUV is independent of body mass:

$$\%ID_I = SUV_i \cdot \frac{m_I}{m_{TB}} \times 100\% \quad \text{Eqn. 2}$$

where SUV_i is the standardized uptake value for mouse organ i , m_I is the mass of human organ I , and m_{TB} is the human total body mass. The $\%ID_I$ at each time point was subsequently multiplied by a corresponding radioactive decay factor. For most tissues, the best fit (Excel 2016 Solver Add-in) of the time-dependent $\%ID_I$ conformed to a bi-exponential clearance model:

$$\%ID_I = Ae^{-\lambda_a t} + Be^{-\lambda_b t} \quad \text{Eqn. 3}$$

where λ_a and λ_b are effective rate constants (i.e. encompassing radioactive decay and biological clearance), A and B are zero-time intercepts of the respective exponential terms, and t is the time post-administration. For the kidneys, a measured increase in activity concentration was observed over the first two hours, and therefore, uptake in this organ was fit with an exponentially rising and then falling model, viz:

$$\%ID_I = A(1 - e^{-\lambda_a t})e^{-\lambda_b t} \quad \text{Eqn. 4}$$

Whole-organ time-integrated activity coefficients (Table 1) were derived from the area under the fitted curves, computed via substitution of Eqn.'s 3 or 4 into Eqn. 1, with the integral taken over the interval $[0, T_D = \infty)$, viz:

$$\tilde{a}(r_s, T_D) = 0.01 \times \left(\frac{A}{\lambda_a} + \frac{B}{\lambda_b} \right) \text{ for clearance only} \quad \text{Eqn. 5}$$

or,

$$\tilde{a}(r_s, T_D) = 0.01 \times \left(\frac{A}{\lambda_b} - \frac{A}{\lambda_a + \lambda_b} \right) \text{ for uptake and clearance} \quad \text{Eqn. 6}$$

S-values (for ^{18}F) for selected organs in the MRKP-AF/-AM phantoms

Table 1: S-values for selected source/target organs in the MRKP-AF and MRKP-AM phantoms.

Organ	S-value (mGy/MBq-s ^{18}F)							
	MRKP-AF				MRKP-AM			
	Liver _s	Pancreas _s	Thyroid _s	Total body _s	Liver _s	Pancreas _s	Thyroid _s	Total body _s
Brain _T	4.49E-08 ± 2.32%	1.87E-08 ± 3.42%	6.05E-07 ± 0.65%	1.41E-06 ± 0.60%	1.91E-08 ± 3.34%	7.71E-09 ± 4.78%	3.49E-07 ± 0.82%	1.12E-06 ± 0.65%
Gallbladder wall _T	1.42E-05 ± 1.86%	6.15E-06 ± 2.71%	2.54E-07 ± 12.28%	1.80E-06 ± 5.59%	6.90E-06 ± 2.28%	7.04E-06 ± 2.22%	8.89E-08 ± 16.64%	1.32E-06 ± 5.51%
Kidneys _T	3.59E-06 ± 0.55%	5.99E-06 ± 0.43%	1.46E-07 ± 2.43%	1.76E-06 ± 0.93%	2.12E-06 ± 0.66%	5.46E-06 ± 0.42%	6.65E-08 ± 3.15%	1.41E-06 ± 0.97%
Liver _T	4.81E-05 ± 0.06%	4.93E-06 ± 0.24%	3.61E-07 ± 0.87%	1.72E-06 ± 0.54%	4.20E-05 ± 0.06%	3.71E-06 ± 0.25%	2.15E-07 ± 1.02%	1.44E-06 ± 0.54%
Lungs _T	2.60E-06 ± 0.37%	1.08E-06 ± 0.54%	1.25E-06 ± 0.52%	1.48E-06 ± 0.59%	1.77E-06 ± 0.38%	8.89E-07 ± 0.51%	1.09E-06 ± 0.48%	1.26E-06 ± 0.54%
Muscle _T	3.35E-07 ± 0.21%	3.33E-07 ± 0.20%	7.23E-07 ± 0.14%	1.47E-06 ± 0.11%	3.75E-07 ± 0.16%	3.76E-07 ± 0.15%	5.59E-07 ± 0.13%	1.18E-06 ± 0.10%
Pancreas _T	4.95E-06 ± 0.77%	4.20E-04 ± 0.06%	1.53E-07 ± 3.81%	1.78E-06 ± 1.52%	3.74E-06 ± 0.81%	3.72E-04 ± 0.06%	9.61E-08 ± 4.25%	1.52E-06 ± 1.53%
SI wall (130-150µm) _T	8.03E-07 ± 5.86%	3.17E-06 ± 3.03%	4.98E-08 ± 23.07%	1.74E-06 ± 4.15%	8.40E-07 ± 5.61%	3.09E-06 ± 2.94%	1.99E-08 ± 35.13%	1.41E-06 ± 4.35%
Spleen _T	1.73E-06 ± 1.09%	5.77E-06 ± 0.62%	2.13E-07 ± 2.89%	1.67E-06 ± 1.40%	1.94E-06 ± 0.98%	8.24E-06 ± 0.50%	9.51E-08 ± 3.84%	1.41E-06 ± 1.44%
Stomach wall (60-100µm) _T	4.86E-06 ± 4.48%	1.36E-05 ± 2.72%	1.94E-07 ± 25.08%	1.67E-06 ± 7.94%	4.83E-06 ± 4.24%	1.37E-05 ± 2.58%	9.55E-08 ± 26.84%	1.54E-06 ± 8.44%
Thyroid _T	3.03E-07 ± 7.96%	1.58E-07 ± 11.44%	3.41E-03 ± 0.06%	1.36E-06 ± 5.13%	1.95E-07 ± 9.12%	8.99E-08 ± 12.44%	2.80E-03 ± 0.06%	1.14E-06 ± 5.02%
Total body _T	1.70E-06 ± 0.05%	1.76E-06 ± 0.05%	1.42E-06 ± 0.05%	1.46E-06 ± 0.07%	1.42E-06 ± 0.05%	1.46E-06 ± 0.05%	1.19E-06 ± 0.05%	1.18E-06 ± 0.07%

Conversion of the MOBY phantom to tetrahedral geometry

The structures that comprise the MOBY phantom are defined mathematically by non-uniform rational basis spline (NURBS) surfaces which are utilized by a command-line application to generate voxel phantoms for Monte Carlo simulations. To configure MOBY for import into PARaDIM, it was converted to tetrahedral geometry via the following procedures.

MOBY was voxelized into a $256 \times 256 \times 800$ array (version 2, “activity” phantom, single frame) with an isotropic voxel size of 145 µm, using all the default organ masses. Organs of interest were defined via a unique label value. The resulting labelmap segments were converted to triangulated polygonal mesh models with 3D Slicer (www.slicer.org), and exported in stereolithography (*.stl) format. The polygon count was reduced using an edge collapse decimation modifier (ratio = 0.1) and slight modifications were made to correct any overlapping or non-manifold/non-watertight surfaces within the open-source computer-aided design software Blender (www.blender.org). The resulting triangulated mesh was converted to a tetrahedral mesh

via 3D constrained Delaunay tetrahedralization with TetGen(4), using the -pAk flag. Finally, the phantom was imported into PARaDIM for self *S*-value calculations. The voxel labelmap-to-tetrahedral mesh conversion procedure employed inevitably introduces small but significant differences in volume between the voxel-defined organs and their tetrahedral analogs. Thus, the mass of the MOBY phantom used in each *S*-value calculation was scaled using PARaDIM's weight scaling function such that the mass of the source organ was equivalent to the values published by Keenan et al.(5) that are used for comparison; this approach is similar to that used by Kostou et al.(6)

Construction of tetrahedral mesh cell phantoms

In order to compare PARaDIM directly with MIRDcell, cells of comparative geometry were modeled with Blender – specifically, the nucleus and outer surface of each cell were modeled using Blender's "icosphere" geometric primitive (4 subdivisions in each case); the radii of the outer surface of each cell were set as 5 μm , and the radii of the nuclei were set as 1, 2, 3, or 4 μm . The cell membranes were modeled from the exterior surfaces using the "solidify" modifier with thickness of +5 nm. Each cell was exported from Blender in the *.stl format and converted to tetrahedral mesh with TetGen using the -pAk flag. Each region of the mesh was materially defined as water (density 1.00 g/cm³), as was the material surrounding the phantom. Finally, each completed phantom was imported into PARaDIM for *S*-value calculations.

Example external source dose calculation with PARaDIM

A hypothetical external radiation exposure scenario was modeled involving a human subject standing in proximity to radionuclide source. The source was chosen as a 55 gallon waste drum filled with an aqueous solution of ¹³¹I (37 MBq homogeneously distributed). A polygonal model was constructed by placing the PSRK-Man(7) phantom and the drum approximately 1 meter apart (center of mass-to-center of mass) into an environment modeled as a rectangular parallelepiped (Fig. 2A,B) in Blender. The "scene" was exported in *.stl format, and tetrahedralized in using the -pAk flag with TetGen(4). Materials were assigned to each tetrahedron region – each human tissue was defined using the original PSRK-/THRK-Man materials, the drum wall was defined as iron with density ρ of 7.8 g/cm³, the drum contents (¹³¹I solution) were defined as water (ρ = 1.0 g/cm³), and the surrounding environment was defined as air (ρ = 0.0012 g/cm³).

The completed phantom was imported into PARaDIM for dose rate calculation. 20 million ¹³¹I photons were simulated from the drum contents (the range of ¹³¹I beta particles is insufficiently long to escape the drum and thus were not simulated). 3D dose map resolution was set to "Medium", and all other PARaDIM parameter defaults were utilized. Uncertainties in mean dose rate for most major organs was < 10% (see Table S1).

Note on use: Source particles are emitted isotropically (i.e. with arbitrary direction) in simulations set up directly with the PARaDIM GUI, and thus external source dose calculations may become

computationally inefficient with increasing source-target distance. Source directionality may be specified by modifying the input files generated by the program for variance reduction.

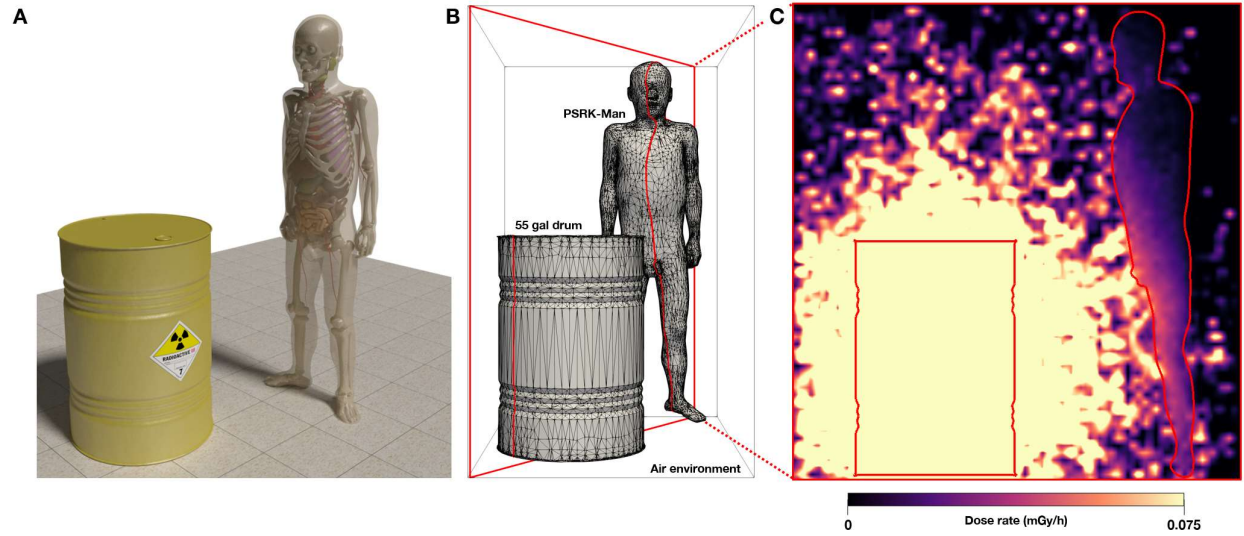


Figure 2: External dose rate calculation with PARaDIM. A) Idealized human external radiation exposure scenario. B) Polygonal mesh “scene” prior to tetrahedralization. C) Slice view of 3D dose map after simulation of 2×10^7 ^{131}I photons with PHITS.

Table 2: Organ-level mean doses from simulation in Supplementary Figure 2.

Organ	Dose Rate (mGy/h)
Esophagus wall	$7.074\text{E-}03 \pm 12.12\%$
Gallbladder wall	$2.269\text{E-}02 \pm 13.03\%$
Large intestine wall	$2.563\text{E-}02 \pm 2.24\%$
Liver	$2.156\text{E-}02 \pm 1.36\%$
Oral mucosa	$1.207\text{E-}02 \pm 30.86\%$
Pancreas	$1.857\text{E-}02 \pm 4.37\%$
Prostate	$3.023\text{E-}02 \pm 10.69\%$
Salivary glands	$1.149\text{E-}02 \pm 7.17\%$
Small intestine wall	$3.302\text{E-}02 \pm 1.56\%$
Stomach wall	$2.533\text{E-}02 \pm 3.52\%$
Blood (circulation)	$1.154\text{E-}02 \pm 5.20\%$
Heart wall	$1.234\text{E-}02 \pm 3.17\%$
Lungs	$1.126\text{E-}02 \pm 1.95\%$
Adrenals	$1.250\text{E-}02 \pm 13.76\%$
Brain	$5.522\text{E-}03 \pm 2.69\%$
Breast tissue	$1.819\text{E-}02 \pm 10.28\%$
Eyes	$1.125\text{E-}02 \pm 14.44\%$
Lens	$1.074\text{E-}02 \pm 90.65\%$
Spleen	$1.443\text{E-}02 \pm 4.24\%$
Thymus	$1.265\text{E-}02 \pm 9.41\%$
Thyroid	$1.111\text{E-}02 \pm 16.68\%$
Bone marrow	$2.191\text{E-}02 \pm 4.80\%$
Cortical bone	$2.259\text{E-}02 \pm 0.50\%$
Kidneys	$1.317\text{E-}02 \pm 3.12\%$
Testes	$5.341\text{E-}02 \pm 5.56\%$
Urinary bladder wall	$3.581\text{E-}02 \pm 5.72\%$
Residual soft tissue	$2.111\text{E-}02 \pm 0.26\%$

References

1. Walt S van der, Colbert SC, Varoquaux G. The NumPy Array: A structure for efficient numerical computation. *Comput Sci Eng*. 2011;13:22-30.
2. Matthew Brett, Michael Hanke, Chris Markiewicz, et al. nipy/nibabel: 2.3.2. Zenodo; 2019.
3. Bolch WE, Eckerman KF, Sgouros G, Thomas SR. MIRD pamphlet No. 21: a generalized schema for radiopharmaceutical dosimetry--standardization of nomenclature. *J Nucl Med*. 2009;50:477-484.
4. Si H. TetGen, a Delaunay-based quality tetrahedral mesh generator. *ACM Trans Math Softw*. 2015;41:11:1–11:36.
5. Keenan MA, Stabin MG, Segars WP, Fernald MJ. RADAR realistic animal model series for dose assessment. *J Nucl Med*. 2010;51:471-476.
6. Kostou T, Papadimitroulas P, Loudos G, Kagadis GC. A preclinical simulated dataset of S - values and investigation of the impact of rescaled organ masses using the MOBY phantom. *Physics in Medicine and Biology*. 2016;61:2333-2355.
7. Yeom YS, Jeong JH, Han MC, Kim CH. Tetrahedral-mesh-based computational human phantom for fast Monte Carlo dose calculations. *Phys Med Biol*. 2014;59:3173-3185.